

# Effects of EDTA and Bicarbonate on U(VI) Reduction by Reduced Nontronite

Shuaidi Wang, Yu Chen,\* Zezhen Pan, Juan Liu, Yuefei Ding, Yuheng Wang, Dong Liu, Songlin Wu, Dafu Hu, Runjie Li, Qingyin Xia, Limin Zhang, and Hailiang Dong\*



Cite This: *Environ. Sci. Technol.* 2024, 58, 23031–23041



Read Online

ACCESS |

Metrics & More

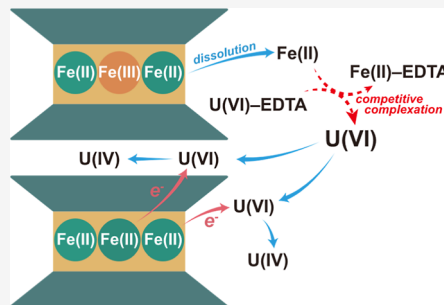


Article Recommendations



Supporting Information

**ABSTRACT:** Widespread Fe-bearing clay minerals are potential materials capable of reducing and immobilizing U(VI). However, the kinetics of this process and the impact of environmental factors remain unclear. Herein, we investigated U(VI) reduction by chemically reduced nontronite (*rNAu-2*) in the presence of EDTA and bicarbonate. U(VI) was completely reduced within 192 h by *rNAu-2* alone, and higher Fe(II) in *rNAu-2* resulted in a higher U(VI) reduction rate. However, the presence of EDTA and NaHCO<sub>3</sub> initially inhibited U(VI) reduction by forming stable U(VI)-EDTA/carbonato complexes and thus preventing U(VI) from adsorbing onto the *rNAu-2* surface. However, over time, EDTA facilitated the dissolution of *rNAu-2*, releasing Fe(II) into solution. Released Fe(II) competed with U(VI) to form Fe(II)-EDTA complexes, thus freeing U(VI) from negatively charged U(VI)-EDTA complexes to form positively charged U(VI)-OH complexes, which ultimately promoted U(VI) adsorption and triggered its reduction. In the NaHCO<sub>3</sub> system, U(VI) complexed with carbonate to form U(VI)-carbonato complexes, which partially inhibited adsorption to the *rNAu-2* surface and subsequent reduction. The reduced U(IV) largely formed uraninite nanoparticles, with a fraction present in the *rNAu-2* interlayer. Our results demonstrate the important impacts of clay minerals, organic matter, and bicarbonate on U(VI) reduction, providing crucial insights into the uranium biogeochemistry in the subsurface environment and remediation strategies for uranium-contaminated environments.



**KEYWORDS:** U(VI) reduction, reduced nontronite *rNAu-2*, U(VI)-EDTA complex, U(VI) species transformation, U(VI)-carbonato complexes

## INTRODUCTION

Uranium is a naturally occurring element with a mean concentration of about 3 mg/kg in the earth crust.<sup>1</sup> Over the past decades, various anthropogenic activities such as mining, milling, fertilizer manufacturing, nuclear testing, disposal of spent nuclear fuels, and nuclear safety accidents<sup>2–4</sup> have contributed to the release of uranium into the environment, leading to widespread contamination. Uranium contamination has emerged as a significant environmental concern on a global scale,<sup>4</sup> as elevated uranium concentrations in the environment pose a serious threat to human health.<sup>5</sup>

The geochemical behavior of uranium in subsurface environments is dependent on multiple factors that include valence state, solubility, and adsorption–desorption behavior.<sup>6</sup> Under the oxic condition, uranium predominantly exists as U(VI), forming highly soluble uranyl ions (UO<sub>2</sub><sup>2+</sup>), which are chemically toxic<sup>8</sup> and exhibit a high mobility in soils and groundwater.<sup>9</sup> Under anoxic conditions, U(VI) can be reduced to sparingly soluble U(IV) (e.g., UO<sub>2</sub>, U<sub>3</sub>O<sub>8</sub>, and U<sub>4</sub>O<sub>9</sub>) through abiotic and biotic processes,<sup>10–14</sup> which can lead to precipitation and immobilization of uranium.<sup>15,16</sup> The reduction of U(VI) to U(IV) can substantially mitigate uranium mobility, which has been used as an effective

remediation strategy for uranium contamination.<sup>17–22</sup> Moreover, recent studies reported that U(V) can form as a transient species during biotic and abiotic reduction of U(VI).<sup>23</sup> U(V) can also either be stabilized at mineral surfaces or be incorporated within both magnetite and green rust.<sup>23</sup>

Numerous studies have observed abiotic reduction of U(VI) by various forms of Fe(II) such as mineral-sorbed Fe(II),<sup>12,24</sup> Fe(II)-containing natural sediments,<sup>25</sup> and Fe(II)-containing minerals,<sup>16,26–28</sup> leading to different forms of reduction products such as coating of UO<sub>2</sub> on a mackinawite surface,<sup>27</sup> UO<sub>2</sub> nanoparticles associated with green rust,<sup>11</sup> adsorbed U(IV) on a magnetite surface,<sup>29</sup> and mineral-incorporated U(V).<sup>30</sup> In particular, Fe-containing clay minerals are ubiquitous in soils, sediments, and sedimentary rocks.<sup>31</sup> Because of their unique properties such as layered structure, high specific surface area, and cation-exchange capacity, clay

Received: September 6, 2024

Revised: December 4, 2024

Accepted: December 6, 2024

Published: December 18, 2024



minerals are often considered as effective adsorbents for heavy metals, including uranium, at various contaminated sites.<sup>31–35</sup> Fe-bearing clay minerals can also undergo redox reactions through biological or nonbiological pathways, while their layered structure remains stable.<sup>31,36</sup> Even after multiple redox cycles, structural Fe in clay minerals can be retained without significant dissolution or recrystallization.<sup>37–39</sup> Studies have demonstrated that reduced Fe-bearing clay minerals play a significant role in the geochemical cycling of various metal pollutants such as U(VI) and Cr(VI).<sup>40–45</sup> Therefore, structural Fe(II) in clay minerals may be a potential reductant that plays a pivotal role in uranium redox reactions.

To our knowledge, there are a few studies focusing on the role of the structural Fe(II) of clay minerals in U(VI) reduction. Zhang et al.<sup>46</sup> utilized chemically reduced nontronite [27% extent of Fe(III) reduction] to reduce U(VI) and observed that U(VI) was hardly reduced in the presence of 30 mM NaHCO<sub>3</sub> at pH 6.8. When the extent of structural Fe(II) in chlorite increased to 85% by microbially mediated Fe(III) reduction, 37% U(VI) was reduced.<sup>47</sup> Similarly, clay minerals with a reduction extent higher than 85% can almost completely reduce U(VI).<sup>48</sup> However, attaining such a high reduction extent of clay minerals under natural conditions may be difficult.<sup>49,50</sup>

Carbonate is commonly present at uranium-contaminated sites<sup>51–53</sup> and can form stable complexes with uranyl, such as UO<sub>2</sub>(CO<sub>3</sub>)<sub>2</sub><sup>2-</sup> and UO<sub>2</sub>(CO<sub>3</sub>)<sub>3</sub><sup>4-</sup>. Although a previous study found that uranyl-carbonato species can be reduced by aqueous Fe(II),<sup>54</sup> the formation of these complexes can decrease the adsorption of U(VI) onto minerals and thus inhibit U(VI) reduction.<sup>51,55,56</sup> However, this effect is poorly understood in the presence of clay minerals. Therefore, research is needed to explore the ability of natural clay minerals [i.e., with environmentally relevant structural Fe(II)] to reduce U(VI) and to investigate the effect of carbonate on U(VI) reduction.

In addition to bicarbonate, organic matter could also influence U(VI) mobility and bioavailability by formation of ternary complexes or aqueous U(VI)-ligand complexes.<sup>57,58</sup> Complexation of uranyl with organic acids (oxalic and citric), natural organic matter (fulvic and humic substances), and synthetic organic acids (EDTA) can facilitate its transport. In particular, EDTA has been widely used in the uranium decontamination process, serving as a typical and powerful chelating agent.<sup>59</sup> As a result, EDTA is commonly observed in natural waters<sup>60</sup> and some radioactively contaminated sites such as Oak Ridge and Hanford sites.<sup>61–63</sup> A previous study has shown that in the absence of minerals, high EDTA concentration can increase U(VI) bioreduction rate because of the formation of aqueous U(IV)-EDTA complexes and thus removal of the passivation effect of U(IV) on the cell surface.<sup>64</sup> Moreover, EDTA can enhance U(VI) bioreduction in the presence of Fe(III)-bearing clay minerals, due to the formation of Fe(II)-EDTA and Fe(III)-EDTA redox couples as electron shuttles.<sup>65</sup>

In addition to its effect on U(VI) bioreduction kinetics, EDTA can also affect the reduction products of U(VI). Zhang et al.<sup>65</sup> observed the formation of an aqueous U(IV)-EDTA complex as a product of U(VI) bioreduction by *Shewanella putrefaciens*. In the presence of Fe-rich clay mineral, U(IV) was sequestered into the solid phase by forming the ternary U(IV)-EDTA-clay surface complex.<sup>65</sup> However, the impact of EDTA on the abiotic reduction of U(VI) by structural

Fe(II) in clay minerals remains unclear. Furthermore, EDTA can dissolve reduced clay minerals and liberate structural Fe(II) to form aqueous Fe(II)-EDTA complexes.<sup>66</sup> The speciation, reduction potentials, and adsorption capacities of Fe(II)-EDTA complexes differ from those of structural Fe(II) in clay minerals,<sup>50,67</sup> all of which can influence the role of Fe(II) in mediating U(VI) reduction. For example, Fe(II)-EDTA complexes can reduce U(VI)-EDTA complexes in the presence of a clay surface,<sup>41,65,91</sup> possibly by changing the ligand fields of Fe(II) and/or U(VI) or bringing aqueous Fe(II) and U(VI) closer together to facilitate the reaction.<sup>65</sup>

The objectives of this study were to (1) examine the ability of structural Fe(II) in reduced nontronite (rNAu-2) to reduce U(VI) under the neutral pH condition; (2) investigate the mechanisms by which bicarbonate and EDTA impact U(VI) reduction by structural Fe(II) in rNAu-2; and (3) determine the resulting products of U(VI) reduction. The results of this study provide new insights into the geochemical and environmental behaviors of uranium and offer a theoretical foundation for uranium remediation.

## MATERIALS AND METHODS

**Materials.** All reagents used in the experiments were of analytical grade. Uranyl acetate (UO<sub>2</sub>(CH<sub>3</sub>COO)<sub>2</sub>·2H<sub>2</sub>O) and EDTA were dissolved in anoxic Milli-Q water (>18.2 MΩ cm) to obtain 10 mM U(VI) and 100 mM EDTA stock solutions, respectively. 10 mM PIPES buffer (pH 7) and 10 mM NaHCO<sub>3</sub> + 10 mM PIPES buffer (hereafter referred to as BP buffer, pH 7) were used to maintain a neutral pH. All solutions were degassed prior to use. Nontronite (NAu-2) was purchased from the Source Clays Repository of the Clay Minerals Society (West Lafayette, Indiana, US), which is an iron-rich smectite with 21.2 wt % Fe content. Details for preparation of NAu-2 are described in Supporting Information Section 1.

**Preparation of Reduced Nontronite (rNAu-2).** A dithionite-citrate-bicarbonate method<sup>68</sup> was used to prepare chemically reduced nontronite (rNAu-2). Briefly, 1 g of freeze-dried NAu-2 was added into 25 mL of citrate-bicarbonate buffer solution and 75 mL of ddH<sub>2</sub>O in order to obtain 10 g/L NAu-2 suspension. The suspension was degassed with high-purity N<sub>2</sub> (99.99%) while being boiled for 30 min and then mixed with sodium dithionite. To achieve two different reduction extents, the mass ratio of NAu-2 to sodium dithionite was set at 1:4 and 1:2. The serum bottles were sealed with rubber stoppers and placed in a constant-temperature water bath at 25 °C for 120 min to achieve 39% reduction and 70 °C for 60 min to achieve 62% reduction [Fe(II)/total Fe ratio]. The resulting rNAu-2 was washed three times with deoxygenated ddH<sub>2</sub>O (>18.2 MΩ cm) to remove any residual reducing agents and negligible amounts of aqueous Fe(II) and subsequently resuspended in 100 mL of anoxic ddH<sub>2</sub>O inside a glovebox for subsequent use (95% N<sub>2</sub> and 5% H<sub>2</sub>, Coy Laboratory Products, Grass Lake, USA).

**U(VI) Reduction by Structural Fe(II) in rNAu-2.** rNAu-2 with two different reduction extents (39%, labeled as 39rNAu-2, and 62%, labeled as 62rNAu-2) was used in the U(VI) reduction experiments to assess their ability to reduce U(VI). To mitigate any difference in adsorption effects caused by varying mass concentrations, equal masses of 39rNAu-2 and 62rNAu-2 suspensions (~2 g/L) were added to Balch tubes to achieve structural Fe(II) concentrations of 1.75 and 2.81 mM, respectively [negligible amounts of aqueous Fe(II) were

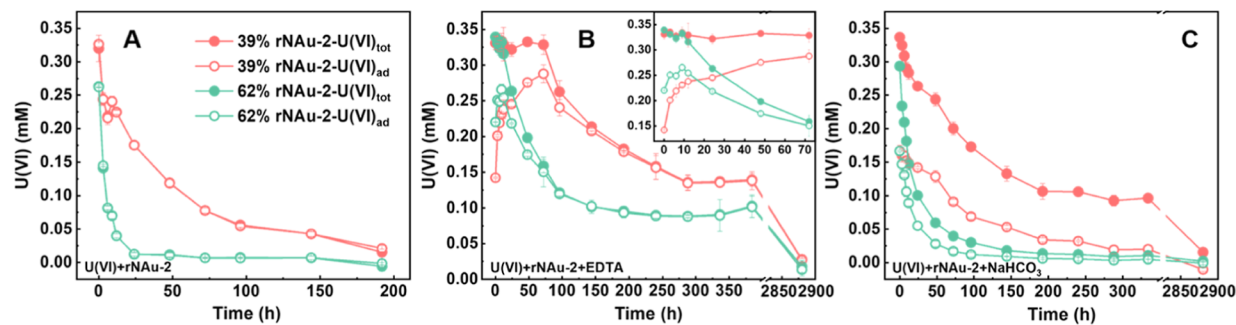


**Figure 1.** Time-course decrease of U(VI) concentration during U(VI) reduction in the presence of (A) only rNAu-2, (B) rNAu-2 and 0.5 mM EDTA, and (C) rNAu-2 and 10 mM NaHCO<sub>3</sub>. Inserted image in (B) is an enlarged view of U(VI) concentration change during initial 0–72 h. U(VI)<sub>tot</sub> represents the total U(VI) concentration. U(VI)<sub>ad</sub> denotes adsorbed U(VI) concentration. The error bars represent standard deviations from triplicate experiments.

removed by three washes]. PIPES buffer (10 mM, pH 7) was dispensed into Balch tubes to maintain a neutral pH. U(VI) stock solution was injected into the tubes to achieve a soluble concentration of 0.35 mM (Table S1). The molar ratio of Fe(II):U(VI) was 4.4 and 7.0 in the 39rNAu-2 and 62rNAu-2 systems, respectively, so that the amount of Fe(II) was in excess. For the EDTA-containing experiment, EDTA stock solution was added to the above clay–U(VI) mixtures to achieve a 0.5 mM EDTA concentration. For the bicarbonate experiment, BP buffer instead of PIPES buffer was injected to achieve a concentration of 10 mM NaHCO<sub>3</sub> (Table S1). The concentrations of EDTA and bicarbonate were chosen for environmental relevance<sup>69,70</sup> and comparisons with earlier studies.<sup>58,71</sup> All experimental setups were performed in triplicate inside a glovebox. At preselected time points, a 0.7 mL subsample was taken from the tubes to analyze concentrations of aqueous U(VI), total U(VI), total Fe(II), and aqueous Fe(II). Nontronite-free controls were also set up, and results showed U(VI) stability over the experimental duration (data not shown).

**Analytical Methods.** Aqueous U(VI) was measured according to the Arsenazo III method<sup>72</sup> with a UV–Vis spectrophotometer (UV-2550, SHIMADZU) after centrifugation of suspension samples (12,000g, 10 min). For total U(VI) concentration [including aqueous U(VI) and mineral-adsorbed U(VI)] measurement, samples were placed in a 200 mM deoxygenized NaHCO<sub>3</sub> solution for 1 h to extract adsorbed U(VI).<sup>46</sup> The mixture was centrifuged (12,000g, 10 min) and filtered (0.22 µm nylon filter) to collect the supernatant. The supernatant was used to measure total U(VI) concentration with the same method.<sup>72</sup> Mineral-adsorbed U(VI) concentration was calculated by the difference between total U(VI) and aqueous U(VI) concentrations. At the end of the experiment (384 h), the total aqueous U concentration [including residual U(VI) and any aqueous U(IV)] was measured by using inductively coupled plasma optical emission spectroscopy (ICP-OES, PerkinElmer, United States). The concentration of aqueous U(IV) was calculated by subtracting the concentration of U(VI) from the total aqueous U concentration.

The 1,10-phenanthroline method<sup>73</sup> was used for measuring the concentrations of total Fe(II) [including structural Fe(II) and aqueous Fe(II)] and total Fe [including Fe(II) and Fe(III)]. The reduction extent of rNAu-2 was calculated by the ratio of the total Fe(II) concentration over the total Fe concentration. Aqueous Fe(II) concentration was measured

using the ferrozine method.<sup>74</sup> Details for U(VI) and Fe(II) measurements are described in Supporting Information Section 2.

At the end of the reaction (384 h), solid-phase characterization was conducted for the representative 62rNAu-2 system. XRD was used to detect the mineralogical changes of rNAu-2. Scanning electron microscopy (SEM) and transmission electron microscopy (TEM) were used to identify the reduced U(VI) products and their spatial association with rNAu-2. The U-oxidation states in the solid products were determined with X-ray photoelectron spectroscopy (XPS). Details for solid-phase characterization are described in Supporting Information Section 3.

Uranium L<sub>III</sub>-edge (17,166 eV) X-ray absorption near-edge structure (XANES) and extended X-ray absorption fine structure (EXAFS) analyses of the solids in the U(VI) + 62rNAu-2 + EDTA experimental system were performed at the end of the experiments (384 h) at the beamline of the Shanghai Synchrotron Radiation Facility, China. Briefly, the solids were collected by centrifugation (3000g, 10 min) and removal of the supernatant in a glovebox. The collected wet solids were loaded into a 3 mm thick slide and covered with a Kapton window. Spectra were collected at room temperature in a N<sub>2</sub>-purged anoxic chamber. Data analysis was performed using the Athena software.<sup>75</sup> Details for X-ray absorption spectroscopy (XAS) analysis are described in Supporting Information Section 4.

**Calculation of U(VI) Speciation.** Visual MINTEQ 3.1<sup>76</sup> was used to calculate the equilibrium speciation of U(VI) under different experimental conditions. Thermodynamic constants for all aqueous reactions including the complexation reactions between U(VI) and EDTA/HCO<sub>3</sub><sup>−</sup> were adopted from the literature (Table S2). Because some uranium species were negligible, only the dominating species were shown in the speciation graphs. Heatmaps of four dominant U(VI) species in the U(VI) + 62rNAu-2 + EDTA experimental system, UO<sub>2</sub>EDTA<sup>2−</sup>, (UO<sub>2</sub>)<sub>2</sub>OHEDTA<sup>−</sup>, (UO<sub>2</sub>)<sub>3</sub>(OH)<sub>5</sub><sup>+</sup>, and (UO<sub>2</sub>)<sub>4</sub>(OH)<sub>7</sub><sup>+</sup>, were generated to depict transformation of U(VI) species under different aqueous Fe(II) and EDTA concentrations. The data for heatmap generation were calculated in Visual MINTEQ 3.1 within the ranges of aqueous Fe(II) concentration from 0 to 0.5 mM and EDTA from 0 to 0.5 mM. The visualization after calculation was performed using the Matplotlib library in Python (version 3.12.3).

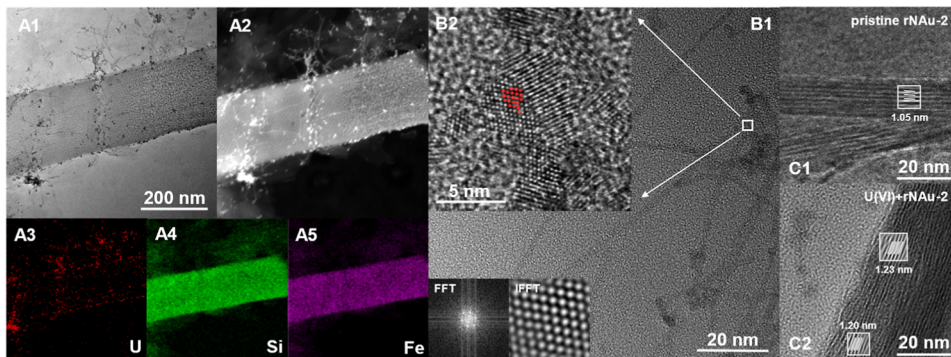


**Figure 2.** TEM morphological characteristics of the U(VI) + 62rNAu-2 samples at the end of reaction (384 h). (A1) TEM images, (A2) HAADF-STEM images, and (A3–A5) U, Si, and Fe elemental maps. (B1) HR-TEM images and (B2) enlarged images of  $\text{UO}_2$  nanoparticles occurring as aggregates and simulated  $\text{UO}_2$  pattern (in red) for the nanoparticles present in the system. The diffractogram (FFT) and the filtered HR-TEM image (IFFT) in the bottom left corner were obtained from the (B2) image and interpreted as crystalline uraninite.  $d_{001}$  spacing of (C1) pristine rNAu-2 and (C2) rNAu-2 in the U(VI) + rNAu-2 samples shown in TEM lattice fringe images.

**Kinetic Analyses.** A zero-order rate model was adopted to fit the kinetic data of U(VI) reduction, as described in previous studies.<sup>50,65</sup> The initial U(VI) reduction rate constants were calculated for the first 72 h because there was a rapid decrease of U(VI) concentration during this period.

## RESULTS AND DISCUSSION

**U(VI) Reduction by rNAu-2.** Both 39rNAu-2 and 62rNAu-2 reduced U(VI) within 192 h (Figure 1A), and U(VI) reduction was coupled with the oxidation of structural Fe(II) in rNAu-2 (Figure S1A). The initial U(VI) reduction rate was higher in 62rNAu-2 than in 39rNAu-2 (21.4 versus 8.86  $\mu\text{M}/\text{h}$ , Table S3). A likely reason was that 62rNAu-2 possessed a lower reduction potential and thus exhibited a stronger reducing capacity for U(VI).<sup>77</sup> However, by the end of the reaction, U(VI) was nearly completely reduced in both treatments.

Previous studies demonstrated the ability of montmorillonite to sorb uranyl ions<sup>10,78–80</sup> and developed models to explain their adsorption behavior.<sup>81</sup> Consistent with these findings, the adsorption of U(VI) on rNAu-2 was observed (Figure 1A). Throughout the entire reaction time, the adsorbed U(VI) concentration (hereafter referred to as  $\text{U}(\text{VI})_{\text{ad}}$ ) was identical to total U(VI) concentration [hereafter referred to as  $\text{U}(\text{VI})_{\text{tot}}$ ] (Figure 1A), suggesting that added U(VI) was entirely adsorbed. Therefore, a potential mechanism for U(VI) reduction by structural Fe(II) in rNAu-2 consists of two steps: U(VI) adsorption to the rNAu-2 surface; subsequent reduction of either edge-adsorbed U(VI) or intercalated U(VI) by octahedral Fe(II) in rNAu-2, which is similar to the interfacial electron transfer mechanism.<sup>48,66,82</sup>

Sorbed U(VI) can be reduced to U(IV) by Fe(II)-bearing minerals, which can result in formation of various reduced U(IV) species such as uraninite, monomeric U(IV), and adsorbed U(IV).<sup>26,29,83</sup> However, in the studies of reduction of U(VI) by reduced clay minerals,<sup>47,48</sup> insufficient attention has been paid to the reduction products. Therefore, the products of the U(VI) + 62rNAu-2 system were investigated in the present study. ICP-OES results showed that total U concentration was nearly identical to total U(VI) concentration, thus suggesting that there was no aqueous U(IV) (Table S3) and reduced U(IV) was sequestered in the solid. Consistently, XRD results indicated that the  $d_{001}$  spacing of rNAu-2 increased from  $\sim 12.4$  to  $\sim 14.3$  Å after the reaction

with U(VI) (Figure S2 and Table S4). A likely explanation is that U(VI) was intercalated into the interlayer of rNAu-2 and the reduction product U(IV) possibly remained there, similar to our previous U(VI) microbial reduction experiments.<sup>84</sup> However, no distinct U(IV) solid was detected in XRD patterns, possibly due to low abundance and incorporation of nanocrystalline U(IV) into the rNAu-2 interlayer.

TEM images and elemental maps for the U(VI) + 62rNAu-2 sample at the end of the experiment (192 h) indicated that uranium was distributed on the rNAu-2 surface (Figure 2A1–A5), consistent with SEM-EDS results (Figure S3). Moreover,  $\text{UO}_2$  nanoparticles were observed in HR-TEM images (Figure 2B1–B2) as the reduction product of the U(VI)-OH hydrolysis species. These nanoparticles were typically less than 3 nm in diameter and present as single particles or clusters (Figure 2B1–B2), similar to previous studies.<sup>26,85</sup> TEM lattice fringe images showed that the  $d_{001}$  spacing of pristine rNAu-2 ranged from 1.05 to 1.19 nm (Figure 2C1). After reaction with U(VI), the  $d_{001}$  spacing of rNAu-2 expanded to 1.20–1.23 nm (Figure 2C2 and Table S5), confirming intercalation of U(IV) into the rNAu-2 interlayer. Compared to the  $d_{001}$  spacings measured by XRD, the  $d_{001}$  spacings of rNAu-2 under TEM were smaller, likely due to layer collapse inside the high vacuum of TEM.

XPS measurement was performed to verify the speciation of uranium in the solid phase. Identical FWHM (full width at half of the maximum) was used to fit the U  $4f_{7/2}$  and U  $4f_{5/2}$  photoelectron peaks. The U  $4f_{7/2}$  peak was located at 380.0 eV (Figure S4A and Table S6) which can be ascribed to  $\text{UO}_2$  solids according to the previously reported values (Table S6).

### U(VI) Reduction by rNAu-2 in the Presence of EDTA

Compared to the rNAu-2 alone (Figure 1A), the addition of EDTA inhibited the rate of U(VI) reduction (Figure 1B). A “lag phase” in total U(VI) concentration was observed in the first 72 h in the U(VI) + 39rNAu-2 + EDTA treatment and the first 9 h in the U(VI) + 62rNAu-2 + EDTA treatment. During this “lag phase”, the initial U(VI) reduction rate was negligible (Figure 1B and Table S3). After the “lag phase”, the  $\text{U}(\text{VI})_{\text{tot}}$  concentration began to decrease. Over a sufficient reaction time (2880 h), both 39rNAu-2 and 62rNAu-2 nearly completely reduced U(VI), which was coupled with the oxidation of structural Fe(II) in rNAu-2 (Figure S1B). As expected, a higher amount of Fe(II) in rNAu-2 enhanced the initial rate of U(VI) reduction (Figure 1B and Table S3).

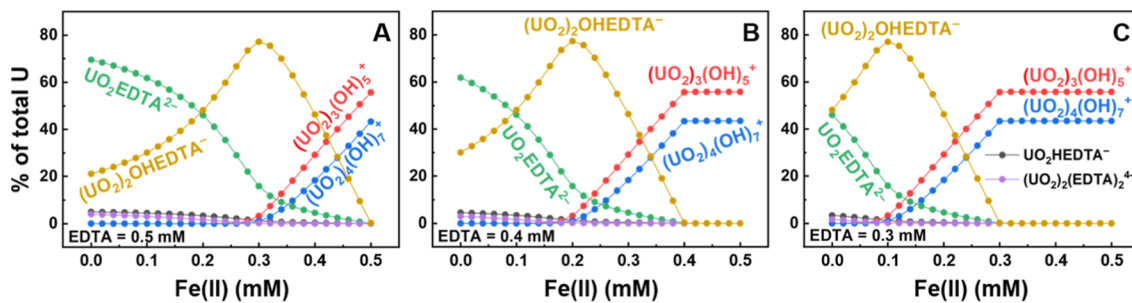


**Figure 3.** U(VI) speciation in the presence of (A) 0.5 mM EDTA, (B) 0.4 mM EDTA, and (C) 0.3 mM EDTA with the increase of aqueous Fe(II) concentration [ $\text{U(VI)}_{\text{initial}} = 0.35 \text{ mM}$ ].

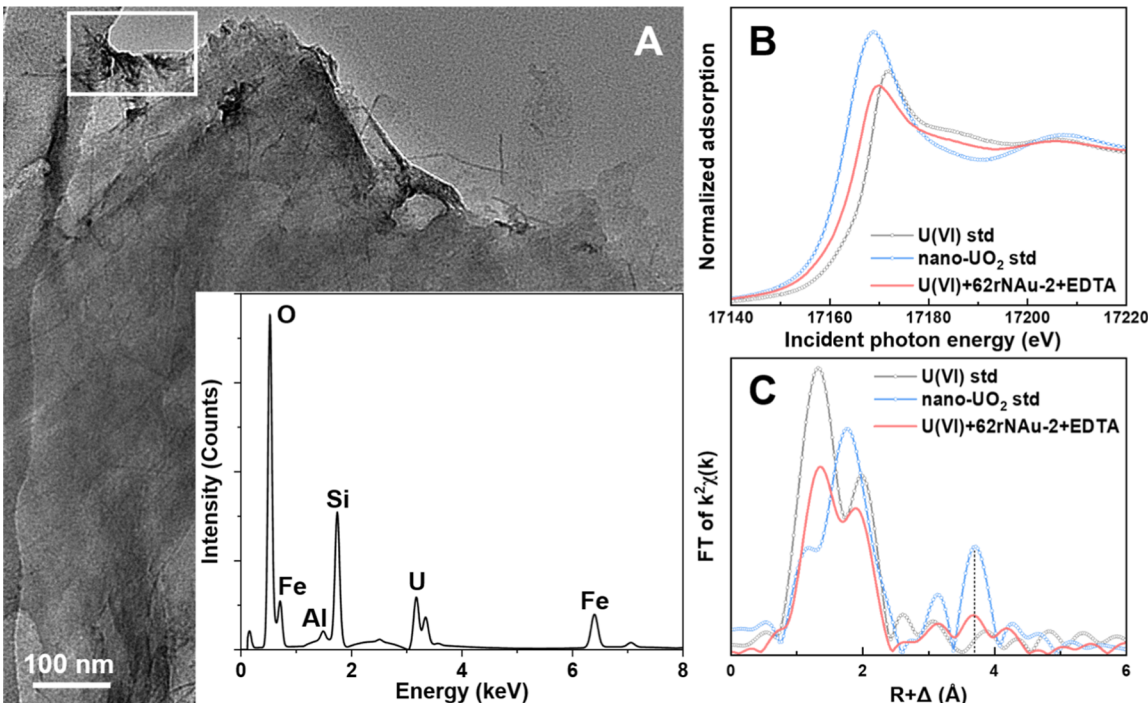


**Figure 4.** (A) TEM image of the solid sample in the  $\text{U(VI)} + 62\text{rNAu-2} + \text{EDTA}$  system and EDS spectrum of the white box area. (B) XANES comparisons to a  $\text{U(VI)}$  standard [ $\text{U(VI)}$  adsorbed to oxidized  $\text{NAu-2}$  in the presence of EDTA] and a  $\text{U(IV)}$  standard (nanoparticulate uraninite).<sup>92</sup> (C) Fourier transforms of the EXAFS data of the solid in this system. Vertical dashed lines note spectral features corresponding to the  $\text{U}-\text{U}$  coordination in the nanouraninite standard.<sup>92</sup>

Unlike the  $\text{U(VI)} + \text{rNAu-2}$  system, where  $\text{U(VI)}$  was completely adsorbed by rNAu-2 throughout the entire reaction period (Figure 1A), only a fraction of  $\text{U(VI)}$  was adsorbed at time zero (Figure 1B). Subsequently, adsorbed  $\text{U(VI)}$  gradually reached a peak, followed by a concomitant decrease in both  $\text{U(VI)}_{\text{ad}}$  and  $\text{U(VI)}_{\text{tot}}$ . As expected, between the two reduced rNAu-2 samples, 62rNAu-2 exhibited greater adsorption and reduction rates of  $\text{U(VI)}$  compared to 39rNAu-2 (Figure 1B), likely due to its lower reduction potential.<sup>50</sup>

Similar to previous study,<sup>66</sup> EDTA partially dissolved rNAu-2 and liberated some structural Fe(II) to the solution (Figure S5A). Relative to the rNAu-2 alone system, the aqueous Fe(II) concentration increased due to the presence of EDTA (Figure S5A,B). To investigate the effect of aqueous Fe(II) on  $\text{U(VI)}$  adsorption and reduction,  $\text{U(VI)}$  speciation was calculated using Visual MINTEQ 3.1.

At the beginning of the reaction, only 0.1 mM aqueous Fe(II) was present (Figure S5), and  $\text{UO}_2\text{EDTA}^{2-}$  was the predominant  $\text{U(VI)}$  species and  $(\text{UO}_2)_2\text{OHEDTA}^-$  secondary

(Figure 3A), likely due to the full availability of EDTA for complexation with  $\text{U(VI)}$ . As the reaction progressed and aqueous Fe(II) concentration increased (Figure S5A), more EDTA-consuming  $\text{UO}_2\text{EDTA}^{2-}$  (per unit of U) was gradually replaced by less EDTA-consuming  $(\text{UO}_2)_2\text{OHEDTA}^-$  species (Figure 3A), likely due to the stronger binding of EDTA with Fe(II) than with  $\text{U(VI)}$ .<sup>86</sup> As the concentration of aqueous Fe(II) further increased, the proportion of  $(\text{UO}_2)_2\text{OHEDTA}^-$  decreased, accompanied by the appearance of EDTA-free  $(\text{UO}_2)_3(\text{OH})_5^+$  and  $(\text{UO}_2)_4(\text{OH})_7^+$  complexes (Figure 3A), likely due to gradual consumption of EDTA by Fe(II). A previous study also reported that  $\text{U(VI)}-\text{EDTA}$  species can undergo decomplexation upon interaction with a magnetite surface, resulting in the formation of an Fe-EDTA complex and hydrated uranyl species.<sup>87</sup>

However, a careful examination revealed that transformation of  $\text{U(VI)}$  species did not depend on Fe(II) availability only. For example, under lower concentration of EDTA (0.4 and 0.3 mM),  $(\text{UO}_2)_3(\text{OH})_5^+$  and  $(\text{UO}_2)_4(\text{OH})_7^+$  became increasingly more important at lower Fe(II) concentrations (Figure 3B,C)

because limited EDTA could be consumed by lower amounts of Fe(II). To illustrate the effects of both Fe(II) and EDTA concentrations on U(VI) speciation, heatmaps were created as a function of Fe(II) and EDTA concentrations (Figure S6).  $\text{UO}_2\text{EDTA}^{2-}$  and  $(\text{UO}_2)_2\text{OHEDTA}^-$  became dominant U(VI) species when the molar ratio of Fe(II):EDTA was below 1 (Figure S6A,B), which corresponded to the beginning of the reaction. When aqueous Fe(II) increased but EDTA decreased,  $(\text{UO}_2)_3(\text{OH})_5^+$  and  $(\text{UO}_2)_4(\text{OH})_7^+$  started to form. When the molar ratio of Fe(II):EDTA was over 1,  $(\text{UO}_2)_3(\text{OH})_5^+$  and  $(\text{UO}_2)_4(\text{OH})_7^+$  became the new predominant U(VI) species (Figure S6C,D), which corresponded to the active U(VI) reduction phase. Therefore, the continuous complexation of EDTA by Fe(II) decreased the amount of EDTA available for complexation by U(VI), and as a result,  $(\text{UO}_2)_3(\text{OH})_5^+$  and  $(\text{UO}_2)_4(\text{OH})_7^+$  species became dominant (Figures 3 and S6), which was consistent with a previous study.<sup>87</sup> This modeled transformation of U(VI) species as a function of the reaction progress presumably converted the charge of the predominant U(VI) species from negative to positive, favoring U(VI) adsorption (i.e., from time 0 to peak adsorption in Figure 1B) and subsequent reduction.

The transformation of predominant U(VI) species as the U(VI) bioreduction progressed could potentially account for the observed “lag phase” in the U(VI) reduction curve (Figure 1B). Compared to the log stability constants of  $\text{UO}_2\text{EDTA}^{2-}$  (13.7) and  $(\text{UO}_2)_2\text{OHEDTA}^-$  (15.4),  $(\text{UO}_2)_3(\text{OH})_5^+$  and  $(\text{UO}_2)_4(\text{OH})_7^+$  have lower stability constants (-15.6 and -21.9, respectively), suggesting that these hydrated species are more reducible than the U(VI)-EDTA complexes.<sup>88-90</sup> Initially, aqueous U(VI)-EDTA complexes were predominant U(VI) species, thus the rate of U(VI) reduction was low (Figure 1B), with electrons predominantly from the Fe(II)-EDTA complex.<sup>41,65,91</sup> As the reaction progressed,  $(\text{UO}_2)_3(\text{OH})_5^+$  and  $(\text{UO}_2)_4(\text{OH})_7^+$  accumulated on the rNAu-2 surface, thus facilitating U(VI) reduction. Once  $\text{UO}_2\text{EDTA}^{2-}$  and  $(\text{UO}_2)_2\text{OHEDTA}^-$  were fully replaced by  $(\text{UO}_2)_3(\text{OH})_5^+$  and  $(\text{UO}_2)_4(\text{OH})_7^+$  species, U(VI) reduction greatly accelerated (Figure 1B), with electrons likely from structural Fe(II) in rNAu-2.

At the end of the reaction (384 h), all reduced U(IV) was sequestered in the solid, as evidenced by the lack of any aqueous U(IV) (Table S3). Elemental maps showed that the surface of rNAu-2 was covered by U-rich materials (Figure S7). Similar to the rNAu-2 alone system, HR-TEM images revealed the presence of a nano- $\text{UO}_2$  phase (Figures 4A and S8A,B). Moreover, XPS measurements revealed the presence of  $\text{UO}_2$  (Figure S4B and Table S6). Compared to pristine rNAu-2 (1.05–1.19 nm), TEM lattice fringe images of rNAu-2 in the presence of EDTA displayed increased  $d_{001}$  spacing (1.06–1.28 nm) after reaction with U(IV) (Figures S8C,D and Table S5), suggesting possible intercalation of reduced U(IV) into the rNAu-2 interlayer. The XRD pattern of the rNAu-2 in the EDTA treatment also confirmed this observation, showing the increase of  $d_{001}$  spacing from 12.5 to 14.8 Å (Figure S2 and Table S4).

Similarly, U L<sub>III</sub>-edge XAS analysis revealed the presence of U(IV) (Figure 4B). Based on the nanouraninite standard, the spectral features corresponding to the U-U coordination were at  $R + \Delta = 3.68$ –3.71 Å (Figure 4C), indicating the formation of nanouraninite in the U(VI) + 62rNAu-2 + EDTA system.<sup>92</sup> However, the amplitude of the U-U spectral feature was lower than that of the nanouraninite standard, which might suggest

that only a fraction of reduced U(IV) was present as nanouraninite, while the remainder may lack the typical  $\text{U}=\text{O}_2=\text{U}$  coordination in uraninite.<sup>92</sup> According to our previous U(VI) bioreduction experiments, the nonuraninite form is possibly a U(IV)-EDTA-NAu-2 ternary complex.<sup>65</sup> However, in the Zhang et al. study,<sup>65</sup> no nano- $\text{UO}_2$  particles were observed because only U(VI)-EDTA complexes [no U(VI)-OH hydrolysis species] were reduced. Therefore, U(VI) speciation is of great importance for the reduction product.

**U(VI) Reduction by rNAu-2 in the Presence of Bicarbonate.** Similar to the case for EDTA, the presence of  $\text{NaHCO}_3$  impeded the rate of U(VI) reduction (Figure 1C). Compared to the initial reduction rates of 8.86 and 21.4  $\mu\text{M}/\text{h}$  by 39rNAu-2 and 62rNAu-2, the initial rates decreased to 5.15 and 12.5  $\mu\text{M}/\text{h}$ , respectively, due to the presence of 10 mM  $\text{NaHCO}_3$  (Table S3). While 62rNAu-2 completely reduced U(VI) within ~300 h, 39rNAu-2 required a much longer time (2880 h) to achieve the same extent (Figure 1C). As expected, U(VI) reduction was coupled with the oxidation of structural Fe(II) in rNAu-2 (Figure S1C).

The inhibition of U(VI) reduction by rNAu-2 in the presence of bicarbonate may be attributed to the formation of uranyl-carbonato complexes. Our thermodynamic calculations showed that  $\text{UO}_2(\text{CO}_3)_3^{4-}$  and  $\text{UO}_2(\text{CO}_3)_2^{2-}$  were the major U(VI) species in the presence of 10 mM  $\text{NaHCO}_3$  and 10 mM PIPES at neutral pH (Figure S9). Uranyl-carbonates are known to lower the U(VI)/U(IV) redox couple and retard the kinetics of U(VI) reduction.<sup>47,93</sup> Additionally, the negatively charged uranyl-carbonate species were unlikely to adsorb to the negatively charged surface of rNAu-2, thereby hindering electron transfer from structural Fe(II) in rNAu-2 to U(VI). In contrast to carbonate-free systems (Figure 1A), a fraction of aqueous U(VI) persisted throughout the entire reaction period until all U(VI) was reduced to U(IV) (Figure 1C), likely in the form of uranyl-carbonato complexes. Nonetheless, throughout the reaction, a fraction of U(VI) was present as an adsorbed form (Figure 1C). Indeed, U(VI) can be absorbed onto sediment<sup>35</sup> and nontronite<sup>46</sup> in the presence of bicarbonate, possibly in the form of a ternary uranyl-carbonato-clay complex.<sup>81</sup> As total U(VI) began to decrease, the concentration of adsorbed U(VI) also declined (Figure 1C), likely through reduction by structural Fe(II) in rNAu-2.

Our results were different from those of Zhang et al.<sup>46</sup> who utilized a chemically reduced nontronite (27% reduction extent) to reduce U(VI) and observed that U(VI) was hardly reduced in the presence of 30 mM  $\text{NaHCO}_3$ . A likely reason was due to kinetic inhibition under high carbonate condition (30 mM)<sup>47</sup> and a relatively low structural Fe(II) in rNAu-2 in their study. A previous study demonstrated that microbially reduced biotite and chlorite with a high Fe(II)/total Fe ratio (>85%) have been shown to reduce >80% U(VI) under low carbonate concentration (0.2 mM).<sup>47</sup> Therefore, the relatively higher structural Fe(II) contents of rNAu-2 (39% and 62%) with lower reduction potentials and moderate bicarbonate levels (10 mM) used in the present study likely resulted in more reduction of U(VI) than that achieved by Zhang et al.<sup>46</sup>

Reduced U(IV) was sequestered in the solid (Table S3) in the form of  $\text{UO}_2$  nanoparticles (Figure S10). XPS results confirmed the presence of  $\text{UO}_2$  (Table S6 and Figure S4C). XPS results also detected 4% unreduced U(VI) remaining at the end of the experiment because U(VI) reduction was not complete when XPS measurement was conducted at 384 h in the 62rNAu-2 system (Figure 1C). In addition, compared to

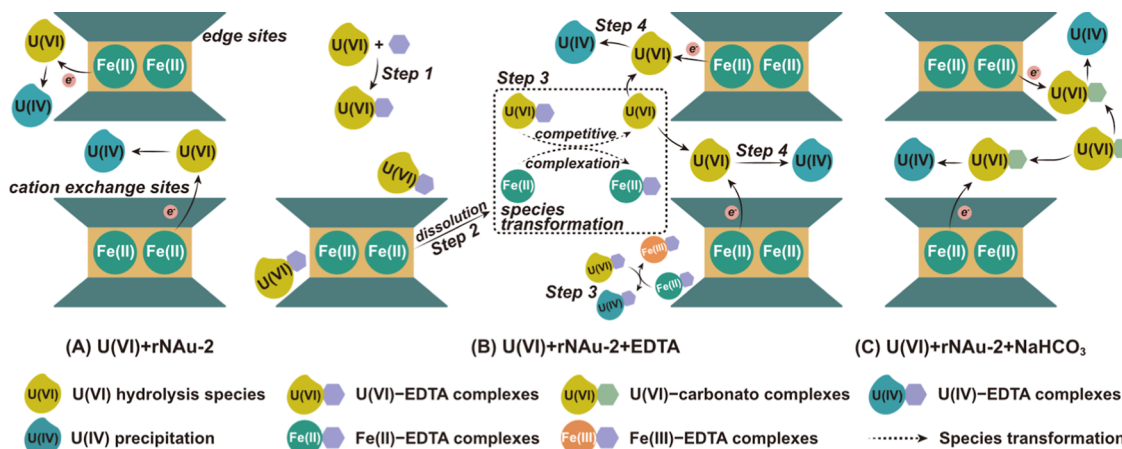


**Figure 5.** Conceptual models of U(VI) reduction by chemically reduced nontronite in the presence of (A) no complexing agents, (B) 0.5 mM EDTA, and (C) 10 mM NaHCO<sub>3</sub>. Steps 1–4 in (B) correspond to the U(VI) reduction mechanism described in the main text. (A) In the absence of complexing agents, U(VI) adsorbs onto the rNAu-2 surface followed by electron transfer from structural Fe(II) in rNAu-2 to U(VI). (B) First, at the early stage, EDTA complexes with U(VI) to form U(VI)-EDTA complexes (step 1), while EDTA promotes rNAu-2 dissolution (step 2). Second, at the intermediate stage, U(VI) species transformation occurs [from U(VI)-EDTA complexes to U(VI) hydrolysis species]. Third, electrons are transferred from Fe(II)-EDTA complexes to U(VI)-EDTA, catalyzed by the rNAu-2 surface (step 3), resulting in a slight reduction of U(VI). Fourth, at the final stage, electrons are transferred from structural Fe(II) to adsorbed U(VI), leading to a major reduction U(VI) (step 4). (C) In the presence of 10 mM NaHCO<sub>3</sub>, U(VI) forms U(VI)-carbonato complexes, which adsorb onto rNAu-2 surfaces and accept electrons from structural Fe(II).

that of pristine rNAu-2, the  $d_{001}$  spacing of rNAu-2 also increased (ranging from 1.16 to 1.36 nm) after reaction with U(VI) in the presence of NaHCO<sub>3</sub> (Table S5 and Figure S10C), indicating some intercalation of the reduced U(IV) within the rNAu-2 interlayer.

**U(VI) Reduction Mechanism.** The identical concentrations of U(VI)<sub>ad</sub> and U(VI)<sub>tot</sub> (Figure 1A) suggested that U(VI) interacted with rNAu-2 via two consecutive processes: adsorption of U(VI) onto rNAu-2 followed by electron transfer from structural Fe(II) to adsorbed U(VI) (Figure 5A). U(VI) adsorption and subsequent reduction can occur at edge sites and the cation-exchange sites of the rNAu-2 interlayer (Figure 5A). Particularly, the adsorption and reduction of U(VI) at the cation-exchange sites can generate reduced U(IV) products to expand the rNAu-2 interlayers.

In the presence of EDTA, the U(VI) reduction mechanism may involve four steps (Figure 5B): Step 1: A fraction of U(VI) forms an aqueous complex with EDTA, hindering adsorption of U(VI), but some EDTA-complexed U(VI) still adsorb to the rNAu-2 surface, forming a U(VI)-EDTA-rNAu-2 ternary complex, similar to the montmorillonite system.<sup>94</sup> Due to the stable nature of U(VI)-EDTA complexes,<sup>88–90</sup> electron transfer from structural Fe(II) in rNAu-2 to these complexes is unfavorable, leading to the “lag phase” of U(VI) reduction (Figure 1B); Step 2: EDTA dissolves rNAu-2 and releases aqueous Fe(II); step 3: Fe(II) and U(VI) compete for complexation with EDTA, resulting in the formation of a soluble Fe(II)-EDTA complex and the transformation of U(VI) species from negatively charged U(VI)-EDTA complexes to positively charged U(VI) hydrolysis species. During this transformation process, electron transfer from aqueous Fe(II)-EDTA complexes to U(VI)-EDTA complexes can occur to form an aqueous Fe(III)-EDTA complex, which may be catalyzed by the rNAu-2 surface,<sup>65</sup> resulting in a slight decrease of U(VI)<sub>tot</sub> concentration during the “lag phase” (Figure 1B); Step 4: The generated U(VI) hydrolysis species adsorb to either the edge sites or the cation-exchange sites of rNAu-2 for reduction

(Figure 5B), similar to the mechanism described in the EDTA-free system (Figure 5A).

The mechanism in the NaHCO<sub>3</sub> system involves dynamic adsorption and reduction of U(VI)-carbonato complexes throughout the entire process (Figure 5C). At the beginning of the reaction, the formation of stable complexes between UO<sub>2</sub><sup>2+</sup> and CO<sub>3</sub><sup>2-</sup> decreases the exposure of U(VI) to the rNAu-2 surface, which results in only a small fraction of U(VI) adsorbed to the rNAu-2 surface (Figure 1C). Structural Fe(II) in rNAu-2 subsequently reduces adsorbed U(VI), precipitating U(IV) onto the rNAu-2 surface or into the interlayer of rNAu-2 (Figure 5C). The residual U(VI)-carbonato complexes continue to adsorb onto the rNAu-2 surface, followed by U(VI) reduction. Although both rNAu-2 and U(VI)-carbonato complexes are negatively charged, U(VI)-carbonato complexes can adsorb onto the rNAu-2 surface by forming complexes at strong ( $\equiv\text{S}^{\text{S}}\text{OUO}_2\text{CO}_3^-$  and  $\equiv\text{S}^{\text{S}}\text{OUO}_2(\text{CO}_3)_2^{3-}$ ) and weak binding sites ( $\equiv\text{S}^{\text{W1}}\text{OUO}_2\text{CO}_3^-$ ).<sup>95</sup> This dynamic adsorption and reduction mechanism is likely responsible for the complete removal of aqueous U(VI) in both the 39rNAu-2 and 62rNAu-2 systems in the presence of bicarbonate (Figure 1C).

## ENVIRONMENTAL IMPLICATIONS

Clay minerals are ubiquitous in soils and sediments, constituting a significant reservoir of iron in natural environments.<sup>31,96,97</sup> They are frequently employed as barriers for disposal of radioactive wastes due to their low hydraulic permeability and high adsorption capacity.<sup>32–34,98</sup> In subsurface anaerobic environments, including uranium-contaminated sites, structural Fe(III) in clay minerals can be reduced by various iron-reducing microorganisms to generate structural Fe(II).<sup>99</sup> Reduced clay minerals exhibit a range of redox potentials depending on the extent of reduction.<sup>50</sup> Due to their reducibility and reusability, reduced iron-containing clay minerals are also utilized as cost-effective and efficient

reductants for remediation of various heavy metals, such as Cr(VI) and Tc(VII).<sup>39,40,44,100,101</sup>

Our study demonstrates that structural Fe(II) in reduced clay minerals has the capacity to reduce U(VI), with the reduction rate of U(VI) depending on the amount of structural Fe(II). The reduction of soluble U(VI) to sparingly soluble U(IV) is an important process to control the mobility of uranium and has been widely used to remove uranium from contaminated sites.<sup>17–19,102</sup> Consequently, future strategies could involve nutrient injection at contaminated sites to enhance the microbial reduction of clay minerals, thereby promoting the reduction and immobilization of U(VI). Compared to the conventional use of oxidized clay minerals as barrier materials for nuclear waste containment, reduced clay minerals not only adsorb U(VI) but also facilitate its reduction. The reduced U(IV) is typically found in solid form or intercalated within clay mineral layers, thereby enhancing uranium stability and minimizing its environmental toxicity.

Previous works have found that EDTA and carbonate can form strong aqueous complexes with U(VI) in groundwater, leading to increased mobility of U(VI) species.<sup>51,55,56,103</sup> Therefore, the immobilization of uranium under EDTA/carbonate-rich conditions should be carefully considered in environmental remediation efforts. In the present study, the presence of EDTA and NaHCO<sub>3</sub> decreases the adsorption of U(VI) on the reduced clay mineral surface and inhibits the reduction rate of U(VI). Nevertheless, U(VI) reduction still occurs under these conditions. Reduced clay minerals can also stabilize the majority of U(VI) as UO<sub>2</sub> nanoparticles or U(IV)–EDTA–clay ternary complexes. Therefore, reduced Fe-bearing clay minerals are desirable materials for long-term remediation of uranium contaminants, even in EDTA/CO<sub>3</sub><sup>2-</sup>-rich environments.

In the presence of EDTA, our findings reveal that Fe(II) released from the dissolution of clay minerals controls the speciation of U(VI) and subsequent reduction in the environment. Both Fe(II) and U(VI) can form complexes with EDTA, resulting in competitive complexation. When the concentration of Fe(II) reaches a certain threshold, it can induce the transformation of negatively charged, highly stable U(VI)–EDTA complexes to positively charged, less stable U(VI) species. This transformation could facilitate the adsorption, reduction, and immobilization of U(VI) by reduced clay minerals. Therefore, future modeling of U(VI) speciation should consider not only the effect of organic complexation on U(VI) speciation but also the effect of other cations that compete with U(VI) for complexation.

Previous studies have demonstrated that both biotic and abiotic U(VI) reduction can proceed via one-electron transfer reactions, forming a U(V) intermediate that disproportionates to generate both U(VI) and U(IV).<sup>104,105</sup> Therefore, future studies should address the role of U(V) in the U(VI) reduction process with reduced clay minerals.

## ASSOCIATED CONTENT

### Supporting Information

The Supporting Information is available free of charge at <https://pubs.acs.org/doi/10.1021/acs.est.4c09492>.

Sections: preparation of clay minerals and chemicals, analytical methods for Fe(II) and U(VI) concentrations, XRD analysis, SEM and TEM observations, XPS analysis, and XAS; tables: experimental setup, stability

constants for U(VI) speciation, reduction rates and final reduction extents of U(VI), and summary of *d*<sub>001</sub> spacings of rNAu-2; and figures: SEM images, XPS spectra, XRD patterns, TEM images, U(VI) speciation modeling, and time-course changes of total Fe(II) and aqueous Fe(II) ([PDF](#))

## AUTHOR INFORMATION

### Corresponding Authors

**Yu Chen** – School of Environment, Tsinghua University, Beijing 100084, China; Phone: 86-010-62784521; Email: [tim1994@163.com](mailto:tim1994@163.com)

**Hailiang Dong** – Center for Geomicrobiology and Biogeochemistry Research, State Key Laboratory of Biogeology and Environmental Geology and School of Earth Sciences and Resources, China University of Geosciences, Beijing 100083, China; [orcid.org/0000-0002-7468-1350](https://orcid.org/0000-0002-7468-1350); Phone: 86-010-82320969; Email: [dongh@cugb.edu.cn](mailto:dongh@cugb.edu.cn)

### Authors

**Shuaidi Wang** – Center for Geomicrobiology and Biogeochemistry Research, State Key Laboratory of Biogeology and Environmental Geology and School of Earth Sciences and Resources, China University of Geosciences, Beijing 100083, China

**Zezen Pan** – Department of Environmental Science and Engineering, Fudan University, Shanghai 200433, China; [orcid.org/0000-0003-1712-3149](https://orcid.org/0000-0003-1712-3149)

**Juan Liu** – The Key Laboratory of Water and Sediment Sciences, College of Environmental Sciences and Engineering, Peking University, Beijing 100871, China; [orcid.org/0000-0002-8456-203X](https://orcid.org/0000-0002-8456-203X)

**Yuefei Ding** – The Key Laboratory of Water and Sediment Sciences, College of Environmental Sciences and Engineering, Peking University, Beijing 100871, China

**Yuheng Wang** – School of Ecology and Environment, Northwestern Polytechnical University, Xi'an 710072, China; [orcid.org/0000-0002-1786-5970](https://orcid.org/0000-0002-1786-5970)

**Dong Liu** – CAS Key Laboratory of Mineralogy and Metallogeny/Guangdong Provincial Key Laboratory of Mineral Physics and Materials, Guangzhou Institute of Geochemistry, Chinese Academy of Sciences, Guangzhou 510640, China

**Songlin Wu** – State Key Laboratory of Urban and Regional Ecology, Research Center for Eco-Environmental Sciences, Chinese Academy of Sciences, Beijing 100085, China; [orcid.org/0000-0001-7469-5253](https://orcid.org/0000-0001-7469-5253)

**Dafu Hu** – Center for Geomicrobiology and Biogeochemistry Research, State Key Laboratory of Biogeology and Environmental Geology and School of Earth Sciences and Resources, China University of Geosciences, Beijing 100083, China

**Runjie Li** – Center for Geomicrobiology and Biogeochemistry Research, State Key Laboratory of Biogeology and Environmental Geology, China University of Geosciences, Beijing 100083, China

**Qingyin Xia** – Beijing Research Institute of Chemical Engineering and Metallurgy, CNNC, Beijing 101149, China

**Limin Zhang** – State Key Laboratory of Microbial Resources, Institute of Microbiology, Chinese Academy of Sciences, Beijing 100101, China

Complete contact information is available at:  
<https://pubs.acs.org/10.1021/acs.est.4c09492>

## Notes

The authors declare no competing financial interest.  
▽ ShuaiDi Wang and Yu Chen are co-first authors.

## ACKNOWLEDGMENTS

Funding for this research was provided by the National Natural Science Foundation of China (No. 42407333 and No. 42107228). We thank Maxim I. Boyanov (ANL) for the nanouraninite standard for XAS analysis and Enyang Liu (SJTU) for her help with analyzing XPS data and performing TEM observation. We are grateful to the Associate Editor and three anonymous reviewers whose comments improved the quality of the manuscript.

## REFERENCES

- (1) Bosshard, E.; Zimmerli, B.; Schlatter, C. Uranium in the Diet: Risk Assessment of its Nephro- and Radiotoxicity. *Chemosphere* **1992**, *24* (3), 309–322.
- (2) Lakanemi, A.-M.; Douglas, G. B.; Kaksonen, A. H. Engineering and kinetic aspects of bacterial uranium reduction for the remediation of uranium contaminated environments. *J. Hazard. Mater.* **2019**, *371*, 198–212.
- (3) Gavrilescu, M.; Pavel, L. V.; Cretescu, I. Characterization and remediation of soils contaminated with uranium. *J. Hazard. Mater.* **2009**, *163* (2–3), 475–510.
- (4) Ma, M.; Wang, R.; Xu, L.; Xu, M.; Liu, S. Emerging health risks and underlying toxicological mechanisms of uranium contamination: Lessons from the past two decades. *Environ. Int.* **2020**, *145*, 106107.
- (5) Atkins, M. L.; Santos, I. R.; Perkins, A.; Maher, D. T. Dissolved radon and uranium in groundwater in a potential coal seam gas development region (Richmond River Catchment, Australia). *J. Environ. Radioact.* **2016**, *154*, 83–92.
- (6) Alam, M. S.; Cheng, T. Uranium release from sediment to groundwater: influence of water chemistry and insights into release mechanisms. *J. Contam. Hydrol.* **2014**, *164*, 72–87.
- (7) Smedley, P. L.; Kinniburgh, D. G. Uranium in natural waters and the environment: Distribution, speciation and impact. *Aquat. Geochem.* **2023**, *148*, 105534.
- (8) Gao, N.; Huang, Z.; Liu, H.; Hou, J.; Liu, X. Advances on the toxicity of uranium to different organisms. *Chemosphere* **2019**, *237*, 124548.
- (9) Grenthe, I.; Stumm, W.; Laaksuharju, M.; Nilsson, A.; Wikberg, P. Redox potentials and redox reactions in deep groundwater systems. *Chem. Geol.* **1992**, *98*, 131–150.
- (10) Chakraborty, S.; Favre, F.; Banerjee, D.; Scheinost, A. C.; Mullet, M.; Ehrhardt, J.-J.; Brendle, J.; Vidal, L.; Charlet, L. U(VI) sorption and reduction by Fe(II) sorbed on montmorillonite. *Environ. Sci. Technol.* **2010**, *44* (10), 3779–3785.
- (11) O'Loughlin, E. J.; Kelly, S. D.; Cook, R. E.; Csencsits, R.; Kemner, K. M. Reduction of uranium(VI) by mixed iron(II)/iron(III) hydroxide (green rust): formation of UO<sub>2</sub> nanoparticles. *Environ. Sci. Technol.* **2003**, *37* (4), 721–727.
- (12) Liger, E.; Charlet, L.; van Cappellen, P. Surface catalysis of uranium(VI) reduction by iron(II). *Geochim. Cosmochim. Acta* **1999**, *63*, 2939–2955.
- (13) Gu, B.; Liang, L.; Dickey, M. J.; Yin, X.; Dai, S. Reductive Precipitation of Uranium(VI) by Zero-Valent Iron. *Environ. Sci. Technol.* **1998**, *32* (21), 3366–3373.
- (14) Schofield, E. J.; Veeramani, H.; Sharp, J. O.; Suvorova, E.; Bernier-Latmani, R.; Mehta, A.; Stahlman, J.; Webb, S. M.; Clark, D. L.; Conradson, S. D.; Ilton, E. S.; Bargar, J. R. Structure of biogenic uraninite produced by *Shewanella oneidensis* strain MR-1. *Environ. Sci. Technol.* **2008**, *42* (21), 7898–7904.
- (15) Egliaud, N.; Miserque, F.; Simoni, E.; Schlegel, M.; Descotes, M. Uranium(VI) interaction with pyrite (FeS<sub>2</sub>): Chemical and spectroscopic studies. *Radiochim. Acta* **2006**, *94*, 651–656.
- (16) Scott, T. B.; Allen, G. C.; Heard, P. J.; Randell, M. G. Reduction of U(VI) to U(IV) on the surface of magnetite. *Geochim. Cosmochim. Acta* **2005**, *69* (24), 5639–5646.
- (17) Williams, K. H.; Long, P. E.; Davis, J. A.; Wilkins, M. J.; N'Guessan, A. L.; Steefel, C. I.; Yang, L.; Newcomer, D.; Spane, F. A.; Kerkhof, L. J.; McGuinness, L.; Dayvault, R.; Lovley, D. R. Acetate Availability and its Influence on Sustainable Bioremediation of Uranium-Contaminated Groundwater. *Geomicrobiol. J.* **2011**, *28* (5–6), 519–539.
- (18) Senko, J. M.; Istok, J. D.; Suflita, J. M.; Krumholz, L. R. In-situ evidence for uranium immobilization and remobilization. *Environ. Sci. Technol.* **2002**, *36* (7), 1491–1496.
- (19) Bargar, J. R.; Williams, K. H.; Campbell, K. M.; Long, P. E.; Stubbs, J. E.; Suvorova, E. I.; Lezama-Pacheco, J. S.; Alessi, D. S.; Stylo, M.; Webb, S. M.; Davis, J. A.; Gianniaro, D. E.; Blue, L. Y.; Bernier-Latmani, R. Uranium redox transition pathways in acetate-amended sediments. *Proc. Natl. Acad. Sci. U.S.A.* **2013**, *110* (12), 4506–4511.
- (20) Huang, J.; Jones, A.; Waite, T. D.; Chen, Y.; Huang, X.; Rosso, K. M.; Kappler, A.; Mansor, M.; Tratnyek, P. G.; Zhang, H. Fe(II) Redox Chemistry in the Environment. *Chem. Rev.* **2021**, *121* (13), 8161–8233.
- (21) Dong, H.; Huang, L.; Zhao, L.; Zeng, Q.; Liu, X.; Sheng, Y.; Shi, L.; Wu, G.; Jiang, H.; Li, F.; Zhang, L.; Guo, D.; Li, G.; Hou, W.; Chen, H. A critical review of mineral-microbe interaction and co-evolution: mechanisms and applications. *Natl. Sci. Rev.* **2022**, *9* (10), nwac128.
- (22) Cui, Q.; Zhang, Z.; Beiyuan, J.; Cui, Y.; Chen, L.; Chen, H.; Fang, L. A critical review of uranium in the soil-plant system: Distribution, bioavailability, toxicity, and bioremediation strategies. *Crit. Rev. Environ. Sci. Technol.* **2023**, *53*, 340–365.
- (23) Roberts, H. E.; Morris, K.; Law, G. T. W.; Mosselmans, J. F. W.; Bots, P.; Kvashnina, K.; Shaw, S. Uranium(V) Incorporation Mechanisms and Stability in Fe(II)/Fe(III) (oxyhydr)Oxides. *Environ. Sci. Technol. Lett.* **2017**, *4* (10), 421–426.
- (24) Regenspurg, S.; Schild, D.; Schäfer, T.; Huber, F.; Malmström, M. E. Removal of uranium(VI) from the aqueous phase by iron(II) minerals in presence of bicarbonate. *Appl. Geochem.* **2009**, *24* (9), 1617–1625.
- (25) Jeon, B.-H.; Dempsey, B. A.; Burgos, W. D.; Barnett, M. O.; Roden, E. E. Chemical reduction of U(VI) by Fe(II) at the solid-water interface using natural and synthetic Fe(III) oxides. *Environ. Sci. Technol.* **2005**, *39* (15), 5642–5649.
- (26) Hyun, S. P.; Davis, J. A.; Sun, K.; Hayes, K. F. Uranium(VI) reduction by iron(II) monosulfide mackinawite. *Environ. Sci. Technol.* **2012**, *46* (6), 3369–3376.
- (27) Veeramani, H.; Scheinost, A. C.; Monsegur, N.; Qafoku, N. P.; Kukkadapu, R.; Newville, M.; Lanzirotti, A.; Pruden, A.; Murayama, M.; Hochella, M. F. Abiotic reductive immobilization of U(VI) by biogenic mackinawite. *Environ. Sci. Technol.* **2013**, *47* (5), 2361–2369.
- (28) Ithurbide, A.; Peulon, S.; Miserque, F.; Beaucaire, C.; Chaussé, A. Interaction between uranium(VI) and siderite (FeCO<sub>3</sub>) surfaces in carbonate solutions. *Radiochim. Acta* **2009**, *97* (3), 177–180.
- (29) Latta, D. E.; Mishra, B.; Cook, R. E.; Kemner, K. M.; Boyanov, M. I. Stable U(IV) complexes form at high-affinity mineral surface sites. *Environ. Sci. Technol.* **2014**, *48* (3), 1683–1691.
- (30) Stagg, O.; Morris, K.; Lam, A.; Navrotsky, A.; Velázquez, J. M.; Schacherl, B.; Vitova, T.; Rothe, J.; Galanew, J.; Neumann, A.; Lythgoe, P.; Abrahamsen-Mills, L.; Shaw, S. Fe(II) Induced Reduction of Incorporated U(VI) to U(V) in Goethite. *Environ. Sci. Technol.* **2021**, *55* (24), 16445–16454.
- (31) Dong, H. Clay-Microbe Interactions and Implications for Environmental Mitigation. *Elements* **2012**, *8* (2), 113–118.

- (32) Uddin, M. K. A review on the adsorption of heavy metals by clay minerals, with special focus on the past decade. *Chem. Eng. J.* **2017**, *308*, 438–462.
- (33) Otunola, B. O.; Ololade, O. O. A review on the application of clay minerals as heavy metal adsorbents for remediation purposes. *Environ. Technol. Innovation* **2020**, *18*, 100692.
- (34) Lee, S. Y.; Tank, R. W. Role of clays in the disposal of nuclear waste: a review. *Appl. Clay Sci.* **1985**, *1*, 145–162.
- (35) Dong, H.; Lu, A. Mineral-Microbe Interactions and Implications for Remediation. *Elements* **2012**, *8* (2), 95–100.
- (36) Dong, H.; Jaisi, D. P.; Kim, J.; Zhang, G. Microbe-clay mineral interactions. *Am. Mineral.* **2009**, *94* (11–12), 1505–1519.
- (37) Zhao, L.; Dong, H.; Kukkadapu, R. K.; Zeng, Q.; Edelmann, R. E.; Penrák, M.; Agrawal, A. Biological redox cycling of iron in nontronite and its potential application in nitrate removal. *Environ. Sci. Technol.* **2015**, *49* (9), S493–S501.
- (38) Fan, Q.; Wang, L.; Fu, Y.; Li, Q.; Liu, Y.; Wang, Z.; Zhu, H. Iron redox cycling in layered clay minerals and its impact on contaminant dynamics: A review. *Sci. Total Environ.* **2023**, *855*, 159003.
- (39) Yang, J.; Kukkadapu, R. K.; Dong, H.; Shelobolina, E. S.; Zhang, J.; Kim, J. Effects of redox cycling of iron in nontronite on reduction of technetium. *Chem. Geol.* **2012**, *291*, 206–216.
- (40) Taylor, R. W.; Shen, S.; Bleam, W. F.; Tu, S.-I. Chromate removal by dithionite-reduced clays: evidence from direct X-ray adsorption near edge spectroscopy (XANES) of chromate reduction at clay surfaces. *Clays Clay Miner.* **2000**, *48*, 648–654.
- (41) Li, R.; Zhang, L.; Chen, Y.; Xia, Q.; Liu, D.; Huang, Y.; Dong, H. Oxidation of Biogenic U(IV) in the Presence of Bioreduced Clay Minerals and Organic Ligands. *Environ. Sci. Technol.* **2024**, *58* (3), 1541–1550.
- (42) Liu, X.; Dong, H.; Yang, X.; Kovarik, L.; Chen, Y.; Zeng, Q. Effects of citrate on hexavalent chromium reduction by structural Fe(II) in nontronite. *J. Hazard. Mater.* **2018**, *343*, 245–254.
- (43) Liu, X.; Dong, H.; Zeng, Q.; Yang, X.; Zhang, D. Synergistic Effects of Reduced Nontronite and Organic Ligands on Cr(VI) Reduction. *Environ. Sci. Technol.* **2019**, *53* (23), 13732–13741.
- (44) Zhang, D.; Liu, X.; Guo, D.; Li, G.; Qu, J.; Dong, H. Cr(VI) Reduction by Siderophore Alone and in Combination with Reduced Clay Minerals. *Environ. Sci. Technol.* **2022**, *56* (17), 12315–12324.
- (45) Chen, Y.; Zhang, L.; Wang, S.; Zeng, Q.; Xia, Q.; Li, R.; Guo, D.; Pan, Z.; Dong, H. Combined effects of humic substances and clay minerals on U(VI) bioreduction. *Geochim. Cosmochim. Acta* **2022**, *338*, 181–198.
- (46) Zhang, G.; Senko, J. M.; Kelly, S. D.; Tan, H.; Kemner, K. M.; Burgos, W. D. Microbial reduction of iron(III)-rich nontronite and uranium(VI). *Geochim. Cosmochim. Acta* **2009**, *73* (12), 3523–3538.
- (47) Brookshaw, D. R.; Patrick, R. A. D.; Bots, P.; Law, G. T. W.; Lloyd, J. R.; Mosselmans, J. F. W.; Vaughan, D. J.; Dardenne, K.; Morris, K. Redox Interactions of Tc(VII), U(VI), and Np(V) with Microbially Reduced Biotite and Chlorite. *Environ. Sci. Technol.* **2015**, *49* (22), 13139–13148.
- (48) Satpathy, A.; Catalano, J. G.; Giamar, D. E. Reduction of U(VI) on Chemically Reduced Montmorillonite and Surface Complexation Modeling of Adsorbed U(IV). *Environ. Sci. Technol.* **2022**, *56* (7), 4111–4120.
- (49) Jaisi, D. P.; Dong, H.; Morton, J. P. Partitioning of Fe(II) in reduced nontronite (NAu-2) to reactive sites: reactivity in terms of Tc(VII) reduction. *Clays Clay Miner.* **2008**, *56* (2), 175–189.
- (50) Luan, F.; Gorski, C. A.; Burgos, W. D. Thermodynamic controls on the microbial reduction of iron-bearing nontronite and uranium. *Environ. Sci. Technol.* **2014**, *48* (5), 2750–2758.
- (51) Abdelouas, A.; Lutze, W.; Nuttall, E. Chemical reactions of uranium in ground water at a mill tailings site. *J. Contam. Hydrol.* **1998**, *34*, 343–361.
- (52) Zhou, P.; Gu, B. Extraction of oxidized and reduced forms of uranium from contaminated soils: effects of carbonate concentration and pH. *Environ. Sci. Technol.* **2005**, *39* (12), 4435–4440.
- (53) Burow, K. R.; Belitz, K.; Dubrovsky, N. M.; Jurgens, B. C. Large decadal-scale changes in uranium and bicarbonate in groundwater of the irrigated western U.S. *Sci. Total Environ.* **2017**, *586*, 87–95.
- (54) Dewey, C.; Sokaras, D.; Kroll, T.; Bargar, J. R.; Fendorf, S. Calcium-Uranyl-Carbonato Species Kinetically Limit U(VI) Reduction by Fe(II) and Lead to U(V)-Bearing Ferrihydrite. *Environ. Sci. Technol.* **2020**, *54* (10), 6021–6030.
- (55) Stewart, B. D.; Mayes, M. A.; Fendorf, S. Impact of Uranyl-Calcium-Carbonato Complexes on Uranium(VI) Adsorption to Synthetic and Natural Sediments. *Environ. Sci. Technol.* **2010**, *44* (3), 928–934.
- (56) Wazne, M.; Korfiatis, G. P.; Meng, X. Carbonate effects on hexavalent uranium adsorption by iron oxyhydroxide. *Environ. Sci. Technol.* **2003**, *37* (16), 3619–3624.
- (57) Novotnik, B.; Chen, W.; Evans, R. D. Uranium bearing dissolved organic matter in the porewaters of uranium contaminated lake sediments. *Appl. Geochem.* **2018**, *91*, 36–44.
- (58) Barger, M.; Koretsky, C. M. The influence of citric acid, EDTA, and fulvic acid on U(VI) sorption onto kaolinite. *Appl. Geochem.* **2011**, *26*, S158–S161.
- (59) Du Bois de Maquille, L.; Renaudin, L.; Gouteland, F.; Jardy, A.; Vial, J.; Thiebaut, D. Determination of ethylenediaminetetraacetic acid in nuclear waste by high-performance liquid chromatography coupled with electrospray mass spectrometry. *J. Chromatogr. A* **2013**, *1276*, 20–25.
- (60) Oviedo, C.; Rodríguez, J. EDTA: The chelating agent under environmental scrutiny. *Quím. Nova* **2003**, *26*, 901–905.
- (61) Means, J. L.; Crerar, D. A.; Duguid, J. O. Migration of Radioactive Wastes: Radionuclide Mobilization by Complexing Agents. *Science* **1978**, *200* (4349), 1477–1481.
- (62) Riley, R. G.; Zachara, J. M. *Chemical Contaminants on DOE Lands and Selection of Contaminant Mixtures for Subsurface Science Research*; U.S. Department of Energy, Office of Energy Research: DOE/ER-0547T; Pacific Northwest National Lab.: Richland, WA (USA), 1992.
- (63) Samuels, W.; Camaioni, D.; Babad, H. *Initial Laboratory Studies into the Chemical and Radiological Aging of Organic Materials in Underground Storage Tanks at the Hanford Complex*; Pacific Northwest Laboratory: Richland, WA, 1994.
- (64) Sheng, L.; Szymanowski, J.; Fein, J. B. The effects of uranium speciation on the rate of U(VI) reduction by *Shewanella oneidensis* MR-1. *Geochim. Cosmochim. Acta* **2011**, *75* (12), 3558–3567.
- (65) Zhang, L.; Chen, Y.; Xia, Q.; Kemner, K. M.; Shen, Y.; O'Loughlin, E. J.; Pan, Z.; Wang, Q.; Huang, Y.; Dong, H.; Boyanov, M. I. Combined Effects of Fe(III)-Bearing Clay Minerals and Organic Ligands on U(VI) Bioreduction and U(IV) Speciation. *Environ. Sci. Technol.* **2021**, *55* (9), 5929–5938.
- (66) Zeng, Q.; Dong, H.; Wang, X. Effect of ligands on the production of oxidants from oxygenation of reduced Fe-bearing clay mineral nontronite. *Geochim. Cosmochim. Acta* **2019**, *251*, 136–156.
- (67) Hudson, J. M.; Luther, G. W.; Chin, Y.-P. Influence of Organic Ligands on the Redox Properties of Fe(II) as Determined by Mediated Electrochemical Oxidation. *Environ. Sci. Technol.* **2022**, *56* (12), 9123–9132.
- (68) Stucki, J. W.; Golden, D. C.; Roth, C. B. Preparation and handling of dithionite-reduced smectite suspensions. *Clays Clay Miner.* **1984**, *32* (3), 191–197.
- (69) Mei, H.; Aoyagi, N.; Saito, T.; Koza, N.; Sugiura, Y.; Tachi, Y. Uranium (VI) sorption on Illite under varying carbonate concentrations: Batch experiments, modeling, and cryogenic time-resolved laser fluorescence spectroscopy study. *Appl. Geochem.* **2022**, *136*, 105178.
- (70) Seeley, F. G.; Kelmers, A. D. *Geochemical Information for the West Chestnut Ridge Central Waste Disposal Facility for Low-Level Radioactive Waste. ORNL-6061*; Oak Ridge National Laboratory: Oak Ridge, Tenn, 1984.
- (71) Rihs, S.; Sturchio, N. C.; Orlandini, K.; Cheng, L.; Teng, H.; Fenter, P.; Bedzyk, M. J. Interaction of uranyl with calcite in the presence of EDTA. *Environ. Sci. Technol.* **2004**, *38* (19), 5078–5086.

- (72) Savvin, S. B. Analytical use of arsenazo III: Determination of thorium, zirconium, uranium and rare earth elements. *Talanta* **1961**, *8*, 673–685.
- (73) Amonette, J. E.; Templeton, J. C. Improvements to the Quantitative Assay of Nonrefractory Minerals for Fe(II) and Total Fe Using 1,10-Phenanthroline. *Clays Clay Miner.* **1998**, *46*, 51–62.
- (74) Stookey, L. L. Ferrozine-A New Spectrophotometric Reagent for Iron. *Anal. Chem.* **1970**, *42*, 779–781.
- (75) Ravel, B.; Newville, M. ATHENA, ARTEMIS, HEPHAESTUS: data analysis for X-ray absorption spectroscopy using IFEFFIT. *J. Synchrotron Radiat.* **2005**, *12*, 537–541.
- (76) Gustafsson, J. P. *Visual MINTEQ 3.1 User Guide*; Royal Institute of Technology: Stockholm, Sweden, 2011.
- (77) Gorski, C. A.; Klüpfel, L. E.; Voegelin, A.; Sander, M.; Hofstetter, T. B. Redox properties of structural Fe in clay minerals: 3. Relationships between smectite redox and structural properties. *Environ. Sci. Technol.* **2013**, *47* (23), 13477–13485.
- (78) Borovec, Z. The adsorption of uranyl species by fine clay. *Chem. Geol.* **1981**, *32*, 45–58.
- (79) Tsarev, S.; Waite, T. D.; Collins, R. N. Uranium Reduction by Fe(II) in the Presence of Montmorillonite and Nontronite. *Environ. Sci. Technol.* **2016**, *50* (15), 8223–8230.
- (80) Pabalan, R. T.; Turner, D. R. Uranium (6+) sorption on montmorillonite: experimental and surface complexation modeling study. *Aquat. Geochem.* **1997**, *2*, 203–226.
- (81) Catalano, J. G.; Brown, G. E. Uranyl adsorption onto montmorillonite: Evaluation of binding sites and carbonate complexation. *Geochim. Cosmochim. Acta* **2005**, *69* (12), 2995–3005.
- (82) Neumann, A.; Olson, T. L.; Scherer, M. M. Spectroscopic evidence for Fe(II)-Fe(III) electron transfer at clay mineral edge and basal sites. *Environ. Sci. Technol.* **2013**, *47* (13), 6969–6977.
- (83) Veeramani, H.; Alessi, D. S.; Suvorova, E. I.; Lezama-Pacheco, J. S.; Stubbs, J. E.; Sharp, J. O.; Dippon, U.; Kappler, A.; Bargar, J. R.; Bernier-Latmani, R. Products of abiotic U(VI) reduction by biogenic magnetite and vivianite. *Geochim. Cosmochim. Acta* **2011**, *75* (9), 2512–2528.
- (84) Zhang, L.; Dong, H.; Li, R.; Liu, D.; Bian, L.; Chen, Y.; Pan, Z.; Boyanov, M. I.; Kemner, K. M.; Wen, J.; Xia, Q.; Chen, H.; O'Loughlin, E. J.; Wang, G.; Huang, Y. Effect of Siderophore DFOB on U(VI) Adsorption to Clay Mineral and Its Subsequent Reduction by an Iron-Reducing Bacterium. *Environ. Sci. Technol.* **2022**, *56* (17), 12702–12712.
- (85) Pan, Z.; Bártová, B.; LaGrange, T.; Butorin, S. M.; Hyatt, N. C.; Stennett, M. C.; Kvashnina, K. O.; Bernier-Latmani, R. Nanoscale mechanism of  $\text{UO}_2$  formation through uranium reduction by magnetite. *Nat. Commun.* **2020**, *11* (1), 4001.
- (86) Blesa, M. A.; Borghi, E. B.; Maroto, A. J.; Regazzoni, A. E. Adsorption of EDTA and iron—EDTA complexes on magnetite and the mechanism of dissolution of magnetite by EDTA. *J. Colloid Interface Sci.* **1984**, *98*, 295–305.
- (87) Kim, Y.; Marciano, M. C.; Kim, S.; Becker, U. Reduction of uranyl and uranyl-organic complexes mediated by magnetite and ilmenite: A combined electrochemical AFM and DFT study. *Geochim. Cosmochim. Acta* **2021**, *293*, 127–141.
- (88) Hummel, W.; Mompean, F. J.; Illemassène, M.; Perrone, J. *Chemical Thermodynamics of Compounds and Complexes of U, Np, Pu, Am, Tc, Se, Ni and Zr with Selected Organic Ligands*; Elsevier Science, 2005.
- (89) Barger, M. L. Investigating the Influence of Organic Acids on Uraninite Solubility and Uranyl Sorption onto Kaolinite. Ph.D. Dissertation, Western Michigan University, 2011.
- (90) Guillaumont, R.; Fanganel, T.; Furger, J.; Grenthe, I.; Neck, V.; Palmer, D. A.; Rand, M. H. *Update on the Chemical Thermodynamics of Uranium, Neptunium, Plutonium, Americium and Technetium*; Elsevier, 2003.
- (91) Kim, S.; Bender, W. M.; Becker, U. Exploring the kinetics of actinyl-EDTA reduction by ferrous iron using quantum-mechanical calculations. *Phys. Chem. Chem. Phys.* **2021**, *23* (9), 5298–5314.
- (92) Boyanov, M. I.; Fletcher, K. E.; Kwon, M. J.; Rui, X.; O'Loughlin, E. J.; Löfller, F. E.; Kemner, K. M. Solution and microbial controls on the formation of reduced U(IV) species. *Environ. Sci. Technol.* **2011**, *45* (19), 8336–8344.
- (93) Behrends, T.; van Cappellen, P. Competition between enzymatic and abiotic reduction of uranium(VI) under iron reducing conditions. *Chem. Geol.* **2005**, *220* (3–4), 315–327.
- (94) Zhou, W.; Wang, J.; He, J.; Yang, X.; Shi, Y.; Wang, X.; Liu, C. Adsorption of U(VI) on montmorillonite in the presence of ethylenediaminetetraacetic acid. *Colloids Surf., A* **2019**, *583*, 123929.
- (95) Marques Fernandes, M.; Baeyens, B.; Dähn, R.; Scheinost, A. C.; Bradbury, M. H. U. VI) sorption on montmorillonite in the absence and presence of carbonate: A macroscopic and microscopic study. *Geochim. Cosmochim. Acta* **2012**, *93*, 262–277.
- (96) Favre, F.; Stucki, J. W.; Boivin, P. Redox properties of structural Fe in ferruginous smectite. A discussion of the standard potential and its environmental implications. *Clays Clay Miner.* **2006**, *54*, 466–472.
- (97) Ito, A.; Wagai, R. Global distribution of clay-size minerals on land surface for biogeochemical and climatological studies. *Sci. Data* **2017**, *4*, 170103.
- (98) Sellin, P.; Leupin, O. X. The Use of Clay as an Engineered Barrier in Radioactive-Waste Management-A Review. *Clays Clay Miner.* **2013**, *61* (6), 477–498.
- (99) Kostka, J. E.; Stucki, J. W.; Nealson, K. H.; Wu, J. Reduction of Structural Fe(III) in Smectite by a Pure Culture of Shewanella Putrefaciens Strain MR-1. *Clays Clay Miner.* **1996**, *44*, 522–529.
- (100) Jaisi, D. P.; Dong, H.; Plymale, A. E.; Fredrickson, J. K.; Zachara, J. M.; Heald, S.; Liu, C. Reduction and long-term immobilization of technetium by Fe(II) associated with clay mineral nontronite. *Chem. Geol.* **2009**, *264* (1–4), 127–138.
- (101) Bishop, M. E.; Dong, H.; Kukkadapu, R. K.; Liu, C.; Edelmann, R. E. Bioreduction of Fe-bearing clay minerals and their reactivity toward pertechnetate (Tc-99). *Geochim. Cosmochim. Acta* **2011**, *75* (18), 5229–5246.
- (102) Lovley, D. R.; Phillips, E. J. P.; Gorby, Y. A.; Landa, E. R. Microbial reduction of uranium. *Nature* **1991**, *350*, 413–416.
- (103) Luo, W.; Gu, B. Dissolution of Uranium-Bearing Minerals and Mobilization of Uranium by Organic Ligands in a Biologically Reduced Sediment. *Environ. Sci. Technol.* **2011**, *45* (7), 2994–2999.
- (104) Vettese, G. F.; Morris, K.; Natrajan, L. S.; Shaw, S.; Vitova, T.; Galanzew, J.; Jones, D. L.; Lloyd, J. R. Multiple Lines of Evidence Identify U(V) as a Key Intermediate during U(VI) Reduction by Shewanella oneidensis MR1. *Environ. Sci. Technol.* **2020**, *54* (4), 2268–2276.
- (105) Molinas, M.; Faizova, R.; Brown, A.; Galanzew, J.; Schacherl, B.; Bartova, B.; Meibom, K. L.; Vitova, T.; Mazzanti, M.; Bernier-Latmani, R. Biological Reduction of a U(V)-Organic Ligand Complex. *Environ. Sci. Technol.* **2021**, *55* (8), 4753–4761.